ChemComm

COMMUNICATION

View Article Online
View Journal | View Issue

Check for updates

Cite this: *Chem. Commun.*, 2019, **55**, 5966

Received 23rd February 2019,
Accepted 3rd April 2019

DOI: 10.1039/c9cc01500k

rsc.li/chemcomm

Published on 05 April 2019. Downloaded by Florida State University on 5/31/2019 6:21:16 PM.

Finding a soft spot for vanadium: a P-bound OCP ligand†

Lauren N. Grant,[a] J. Krzystek,[b] Balazs Pinter,[c] Joshua Telser,[d] Hansjörg Grützmacher[e] and Daniel J. Mindiola*[a]

Transmetallation studies with the phosphaethynolate ion, $[OCP]^-$, have largely resulted in coordination according to classical Lewis acid–base theory. That is, for harder early transition metal ions, O-bound coordination has been observed, whereas in the case of softer late transition metal ions, P-bound coordination predominates. Herein, we report the use of a V(III) complex, namely [(nacnac)VCl(OAr)] (1) (nacnac$^-$ = [ArNC(CH$_3$)]$_2$CH; Ar = 2,6-^{i}Pr$_2$C$_6$H$_3$), to transmetallate $[OCP]^-$ and bind *via* the P-atom as [(nacnac)V(OAr)(PCO)] (2), the first example of a 3d early transition metal that binds $[OCP]^-$ *via* the P-atom. Full characterization studies of this molecule including HFEPR spectroscopy, SQuID measurements, and theoretical studies are presented.

The ligand class formulated as $[XCE]^-$, where X = chalcogen (O, S, Se) and E = pnictogen (N, P, As), has long featured the ubiquitous, ambidentate $[OCN]^-$ and $[SCN]^-$ ligands.[1] A facile and bulk synthesis of another $[XCE]^-$ ligand, the phosphaethynolate ion, $[OCP]^-$,[1] has lately been developed, opening a gateway to new chemistry given the softer and more polarizable nature of phosphorous in comparison with the aforementioned nitrogen congener.[1] In recent years $[OCP]^-$ has demonstrated impressive reactivity ranging from organic transformations to new p-, d-, and f-block complexes, which also showcases its ambidentate ability. Thus, in "harder" and electropositive metal ions, O-bound coordination of $[OCP]^-$ is expected to be dominant,[3,4l–o] whereas in highly electron-rich W(0) and low-valent Ge, the coordination is *via* the P-atom.[4a–f] However, the reactivity of $[OCP]^-$ with early transition metals remains limited.[2–4] As steps in this direction, we recently reported the divergent reactivity of sodium phosphaethynolate, [Na(OCP)(1,4-dioxane)$_{2.5}$], with early transition metals.[2,3] In particular, reaction with Ti(III) and Sc(III) halide precursors afforded, respectively, a decarbonylated species having a $[Ti_2P_2]$ core, and reductive coupling of $[OCP]^-$, to yield a diphosphaethynolate ion, $[OCPPCO]^{4-}$, stabilized by two Sc(III) ions (Scheme 1).[2,3] Based on Hard/Soft Acid–Base (HSAB) theory we inquired if we could achieve the uncommon phosphaketenyl binding mode[4q] (P-bound) to an early-transition metal ion. Although one anticipates that making the metal electron-rich should promote P-binding to the now softer metal site, reductive decarbonylation readily prevents identification of such putative species.[4h] Herein, we show how a vanadium(III) precursor can allow us to isolate and fully characterize a high-spin P-bound vanadium(III)–PCO complex that is resistant to decarbonylation. In addition to structural characterization and DFT analysis, we report high-frequency and -field EPR (HFEPR) spectral data and solid-state magnetization data in accord with such a species being a high-spin d^2 complex (S = 1 ground state).

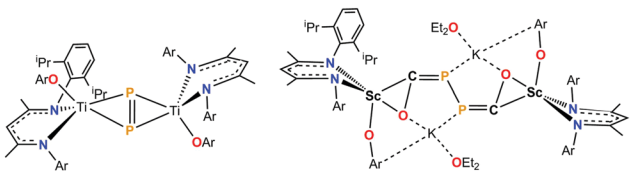

Scheme 1 Dinuclear, early-transition metal complexes prepared from trivalent precursors followed by reductive decarbonylation (Ti, left) or reductive coupling (Sc, right) of the diphosphaethynolate ion $[OCP]^-$. Ar represents 2,6-^{i}Pr$_2$C$_6$H$_3$.

Following the procedure used for previously reported Ti and Sc complexes, [(nacnac)VCl(OAr)][5] (**1**) (nacnac$^-$ = [ArNC(CH$_3$)]$_2$CH; Ar = 2,6-^{i}Pr$_2$C$_6$H$_3$) was treated with 1 equiv. of [Na(OCP)(diox)$_{2.5}$][1a] (diox = 1,4-dioxane) as a slurry in toluene at room temperature, and the mixture was allowed to stir for 12 h. Examination of the crude reaction mixture revealed the formation of a new species displaying broadened resonances in the ^{1}H NMR spectrum in the 0.5 to 9 ppm range, whereas the paramagnetic resonances attributable to the starting material **1** were no longer present (see Fig. S1, ESI†).[6]

[a] *Department of Chemistry, University of Pennsylvania, Philadelphia, PA 19104, USA. E-mail: mindiola@sas.upenn.edu*
[b] *National High Magnetic Field Laboratory, Florida State University, Tallahassee, FL 32310, USA*
[c] *Department of Chemistry, Universidad Técnica Federico Santa María, Valparaíso, 2390123, Chile*
[d] *Department of Biological, Physical and Health Sciences, Roosevelt University, Chicago, IL 60605, USA*
[e] *Department of Chemistry and Applied Biosciences, ETH Zürich, Vladimir-Prelog Weg1, Hönggerberg, Zürich, 8093, Switzerland*

† Electronic supplementary information (ESI) available. CCDC 1890542 for **2**. For ESI and crystallographic data in CIF or other electronic format see DOI: 10.1039/c9cc01500k

This journal is © The Royal Society of Chemistry 2019

Published on 05 April 2019. Downloaded by Florida State University on 5/31/2019 6:21:16 PM.

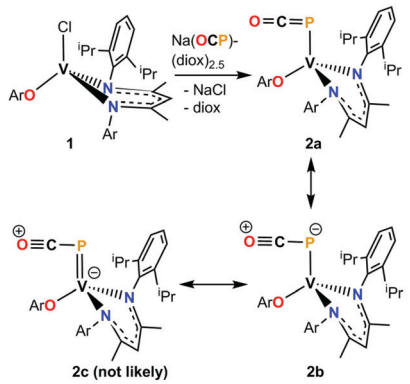

Scheme 2 Synthesis of complex **2** from **1** (which is prepared from [(nacnac)VCl_2] by reaction with NaOAr).[5] In all instances, Ar represents 2,6-$^{i}Pr_2C_6H_3$. Three possible canonical forms for **2** are presented, of which **2c** is unlikely based on a combination of metrical parameters and theoretical studies.

Although [Na(OCP)$(diox)_{2.5}$] is not soluble in toluene, it is critical that coordinating solvents such as THF be avoided in the protocol since their use results in rapid decomposition of the product. To characterize the identity of the green material formed in this reaction, a concentrated toluene solution was stored for 16 hours at −35 °C to afford green crystals of [(nacnac)V(OAr)(PCO)] (**2**) (Scheme 2) in 89% yield, for which V–P, as opposed to V–O, connectivity was unambiguously confirmed by single crystal X-ray diffraction (XRD) studies (Fig. 1 and Fig. S3, ESI†).[6]

In addition to XRD confirming the atypical binding mode of $[OCP]^-$ to an early-transition metal center, the coordination geometry of the phosphaethynolato ligand reveals an unusual angle due to significant pyramidalization at the phosphorus atom. In contrast to [(nacnac)Sc(OAr)(OCP)(THF)], where, much like the [Na(OCP)$(diox)_{2.5}$] precursor, the $[OCP]^-$ ion binds through the O-atom in a near-linear fashion with the metal center (∠Sc–O–C of 170.89(2)°) with no other exceptional metrical features, the binding mode of $[OCP]^-$ in **2** is essentially perpendicular to the V–P vector, with a ∠V–P–C of 85.93(5)°. This resembles the binding mode of $[OCP]^-$ with late transition metals such as Re (92.6)° and Au (86.2)°.[4a–c] However, the linearity within the $[OCP]^-$ moiety is still maintained in **2** with a P1–C42–O2 angle of 176.31(1)°. A strong ν(C–O) of 1876 cm^{-1} was seen in the IR spectrum (Fig. S2, ESI†),[6] which is similar to the other few known P-bound $[OCP]^-$ moieties involving late transition metals (Co: 1851 cm^{-1}, Re: 1885 cm^{-1}).[4a,b] Notably, the long V–P bond distance of 2.4502(4) Å significantly diverges from those of other P-bound examples of $[OCP]^-$ to 3d metals such as Co–P: 2.263(1) Å and Cu–P: 2.2244(5) Å.[4b] It is also significantly longer than known vanadium phosphinidene complexes (V–P: 2.14–2.19 Å).[7–9] Perhaps the most notable metrical parameter in the solid-state structure of **2** is the P–C bond length of 1.6360(18) Å, which falls more in the range of a single or double bond, but is clearly longer than that of the precursor $[Na(OCP)(dme)_2]_2$, 1.575(3) Å and 1.589(3) Å.[1a] The C–O bond length of 1.174(2) Å is commonly observed for systems possessing double and triple bonds, and is slightly shorter than the aforementioned precursor, 1.203(4) Å and 1.213(3) Å.[1a] In accordance with these observations, Scheme 2 presents the most reasonable canonical structures to be considered. As shown in Scheme 2, structures **2a** and **2b** are each quite reasonable based on the P–C and C–O distances and will be discussed further in light of computational studies. The metallophosphaketene resonance **2c** is the least likely, on the basis of metrical parameters, chiefly the longer V–P distance, observed in the solid-state structure. Further characterization of **2** by the Evans NMR spectroscopic method confirmed the S = 1 nature of **2** in toluene solution at room temperature, *i.e.*, a high-spin d^2 complex with a μ_{eff} = 2.47. The solid-state magnetic behavior of **2** was also probed using DC susceptibility. As shown in Fig. S4 (ESI†),[6] **2** clearly has an S = 1 ground state with a sharp decrease in χT below ∼20 K due to the effect of zero-field splitting (zfs). The phenomenon of zfs is key to the desired behavior of d-block single ion magnets; however, this property is not the goal here. However, the zfs itself, chiefly the magnitude and sign of the axial zfs parameter, D, provides valuable information on electronic structure, such as the nature of the frontier MOs and the accessibility of electronically excited states.[10] It was not possible *via* fitting to distinguish between a positive and a negative value for D, which is a common phenomenon.[10–13] As a result, the possibility of rhombic zfs (E parameter) was not explored. Our fit suggested a magnitude of D on the order of 4 cm^{-1}, exhibiting temperature independent paramagnetism (TIP), which is qualitatively the consequence of the contribution of thermally populated spin triplet excited states not accounted for by the simple S = 1 spin Hamiltonian (sH) employed.[11,12]

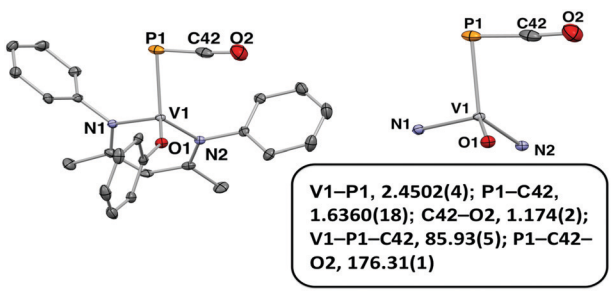

Fig. 1 Molecular structure of complex **2**, with nacnac ^{i}Pr groups and all hydrogen atoms omitted for clarity (left); expansion of the PCO^- ligand coordinated to the $[(nacnac)V(OAr)]^+$ scaffold showing only the first coordination sphere of the latter (right). All thermal ellipsoids are shown at the 50% probability level. Bond lengths are reported in angstroms (Å) and angles in degrees (°).

To further address the electronic structure of complex **2**, HFEPR spectra were recorded on a ground polycrystalline sample, analogous to that used for the DC susceptibility measurements. The spectra produced by **2** could be recognized as originating from a triplet (S = 1) state with moderate zfs. The number and intensities of turning points could indeed be readily simulated. An HFEPR spectrum at a relatively low frequency (113 GHz, Fig. S5, ESI†)[6] provided the best representation of a triplet powder pattern,[14] but the frequency was too low to unambiguously determine the absolute sign of D.[14] For this reason, a spectrum at a higher frequency (257 GHz, Fig. 2) was needed. The relative amplitudes of the experimental turning points belonging to the transitions originating from the $|S, M_S\rangle = |1, 0\rangle$ spin sublevel are higher than those originating from one of the $|1, \pm1\rangle$ sublevels, which clearly shows the positive sign of D. To determine the full set of

Published on 05 April 2019. Downloaded by Florida State University on 5/31/2019 6:21:16 PM.

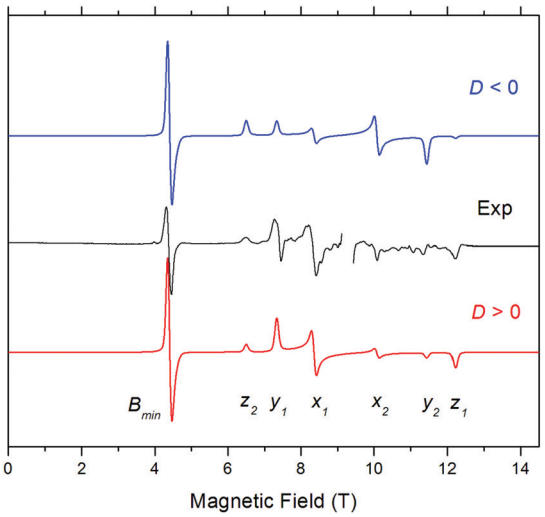

Fig. 2 An HFEPR spectrum of **2** recorded at 10 K and 257 GHz (black trace). A V(IV) impurity signal at g = 1.98 (~9.3 T) has been removed. Coloured traces are simulations using sH parameters: S = 1, $|D|$ = 2.62 cm^{-1}, $|E|$ = 0.36 cm^{-1}, g_x = 1.96, g_y = 1.94, and g_z = 1.95. The particular turning points are labelled by the canonical direction (x, y, z) of the magnetic field with respect to the **D** tensor and have subscript 1 for those that belong to the transition originating from the $|S, M_S\rangle$ = $|1, 0\rangle$ spin sublevel, while those with subscript 2 originate from one of the $|1, \pm1\rangle$ sublevels.

S = 1 sH parameters, particularly the g values and rhombic parameter E, a complete field-frequency dependence of the HFEPR transitions was recorded.[15] Such a dependence is shown in Fig. 3, from which the sH parameters can be extracted with high precision and accuracy as: D = +2.60(1) cm^{-1}, $|E|$ = 0.346(5) cm^{-1}, g_x = 1.962(5), g_y = 1.938(5), and g_z = 1.953(5).

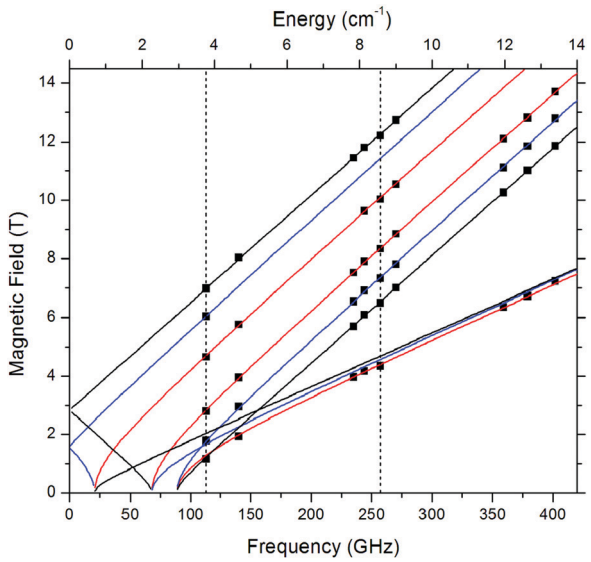

Fig. 3 A 2D field *vs.* frequency (energy) plot of HFEPR spectral turning points in **2**. Squares are experimental data; curves were simulated using sH parameters as in the text. Red curves: turning points with the magnetic field parallel to the x-axis of the zfs tensor; blue curves: $B_0 \| y$; black curves: $B_0 \| z$. The two vertical dashed lines indicate the frequencies at which the spectra shown in Fig. S5, ESI,† and Fig. 2, respectively, were recorded.

The sH parameters obtained for **2** can be put into the context of those for related species inasmuch as possible. We have previously employed HFEPR to extract the zfs of a V(III) complex related to **2**, [(nacnac)V(N$_3$)(Ntol$_2$)] (tol = 4-MeC$_6$H$_4$) (**3**), which gave D = −1.65 cm^{-1} and $|E|$ = 0.20 cm^{-1}.[16] This previously studied complex shares the nacnac ligand with **2** and is likewise four-coordinate. That the D values for two such [(nacnac)-V^{III}(X)(Y)] complexes (X = $^-$OAr, Y = $^-$PCO in **2**; X = N$_3^-$, Y = $^-$NR$_2$ in **3**) are of opposite sign indicates the difficulty in generalizing the correlation between zfs and the coordination sphere of a metal ion. An ideally tetrahedral d^2 complex should exhibit no zfs, and homoleptic four-coordinate V(III) complexes such as [V(Ar$^{n\mathrm{Cl}}$)$_4$]$^-$ (Ar$^{n\mathrm{Cl}}$ = C$_6$Cl$_5$, 2,4,6-trichlorophenyl, or 2,6-dichlorophenyl) indeed exhibit smaller magnitude zfs values (0.45 ≤ $|D|$ ≤ 0.59 cm^{-1}) than those observed here for heteroleptic complexes,[17] which is expected based on ligand-field theory for pseudo-tetrahedral d^2 complexes.[18] Clearly, a greater database on zfs in four-coordinate V(III) complexes is needed to further evaluate the magnitude and absolute sign of the zfs in **2**. Moreover, the unusual [PCO]$^-$ coordination means that **2** may even be distinct amongst the mononuclear [(nacnac)V^{III}(X)(Y)] complexes.

To elucidate the electronic structure of **2** in detail and reveal the most likely canonical resonance of the [OCP]$^-$ ligand in **2**, we turned to DFT (B3LYP/def2-TZVP(-f)).[6] These calculations on non-truncated models revealed an equilibrium structure for **2** with metrics in good agreement with the X-ray structural parameters. For example, the quasi-perpendicular ∠V–P–C angle (85.0°) and distances V–P (2.46 Å), P–C (1.66 Å) and C–O (1.17 Å) are well reproduced by these DFT calculations, substantiating the method of calculation. To characterize the bending and bonding of the V–PCO motif in **2**, we used quasi-restricted orbitals (QROs). QROs offer a reliable and intuitive description of the unrestricted wavefunctions (with different α and β orbital subsets) through a conceptual picture resembling that of the restricted open-shell solution. The two singly occupied QROs of **2**, d$_{z^2}$ and d$_{x^2-y^2}$ (Fig. 4; see also Fig. S6, ESI†),[6] unmistakably reveal metal-centered unpaired electrons without notable delocalization to any of the ligands, *i.e.*, a d^2 V(III) center, conforming to a spin density of 1.96 calculated for the vanadium of **2** using the Löwdin method, and consistent with the HFEPR results. Close inspection of the orbital entitled π_{PCO} + d$_{xz}$ in Fig. 4 unveils the vanadium–PCO σ bond, which is the main V–PCO interaction, as originating from the overlap of one of the π orbitals of the [OCP]$^-$ fragment and a σ-type vanadium d orbital, d$_{xz}$, in the quasi-tetrahedral arrangement of **2**.

The spatial characteristics of this PCO π-bond account for most of the striking structural features observed, such as the elongated P–C and significantly shortened C–O distances in the [OCP]$^-$ ligand. These spatial features indicate that this π_{PCO} orbital has bonding character along the P–C vector and anti-bonding character along the C–O vector, which, under normal circumstances like in the free ligand, lead to a short P–C bond and a long C–O bond (*i.e.* to P≡C–O$^-$ formally). In **2**, however, electron donation takes place from this π_{PCO} orbital to the vanadium, witnessed by the π_{PCO} + d$_{xz}$ molecular orbital in Fig. 4, from which partial depopulation of π_{PCO} results in

 This journal is © The Royal Society of Chemistry 2019

Published on 05 April 2019. Downloaded by Florida State University on 5/31/2019 6:21:16 PM.

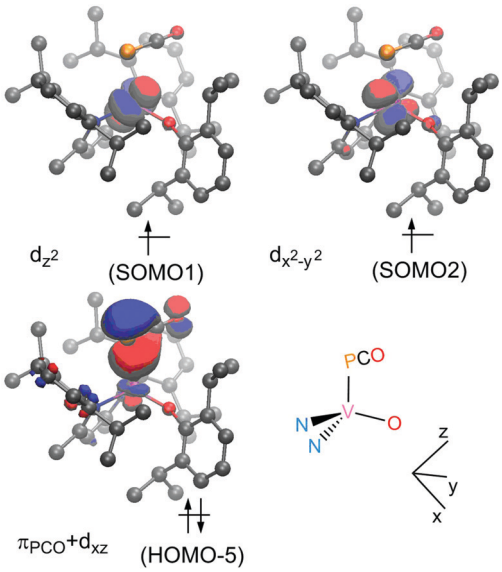

Fig. 4 Relevant QROs of triplet **2**. The upper two QROs represent the V-centered unpaired electrons, while HOMO−4 depicts the V–P σ interaction. The isodensity values are ±0.04.

diminished attraction and diminished repulsion along the P–C and C–O axes. The latter effects lead to the weakening of the P–C bond and strengthening of the C–O bond relative to that of free $[OCP]^-$, consistent with the structural features in **2**. Also, due to the polarization of this PCO π-bond towards the phosphorous atom, ∠V–P–C deviates from angles typical of side-on or κ^2 coordination and towards perpendicular κ^1-type binding at P. As a result, this MO analysis implies that the formal electronic structure of $[OCP]^-$ changes from P≡C–O$^-$ (in the free ligand) to $^-$P=C=O upon binding to V(III) and, concomitantly, that the Lewis structure of **2** is dominated by resonance **2a** (Scheme 2). The $[OCP]^-$ structural motif is further supported by the Mayer bond indices of 1.75 and 2.06 calculated for P=C and C=O, respectively, in **2**.

In summary, we report the first example of the $[OCP]^-$ reagent binding to a highly electropositive 3d early transition metal, vanadium(III), *via* the P-atom, and the unexpected ∠V–P–C of 85.93(5)°. Our perception is that the HSAB concept's "soft–soft" argument, which can be translated into the MO framework as the electron-rich V(III) having a better orbital energy match with phosphorous orbitals than with oxygen orbitals, explains the site-selective P-binding of $[OCP]^-$ to vanadium(III). On the other hand, the almost perpendicular binding and elongated/shortened P–C/C–O bonds of $[OCP]^-$ can be best rationalized, as detailed above, through the characteristics of the π_{PCO} orbital that forms the σ interaction with the vanadium center (Fig. 4).

For funding, we thank the University of Pennsylvania and the Chemical Sciences, Geosciences, and Biosciences Division, Office of Basic Energy Sciences, Office of Science, U. S. DOE (DEFG02-07ER15893 to D. J. M., synthesis and characterization). L. N. G. thanks NSF GRFP for funding. Part of this work was performed at NHMFL, which is supported by the NSF award DMR-1644779 and by the State of Florida. We thank Riccardo Suter for providing $[Na(OCP)(dioxane)_{2.5}]$, Dr Andrew Ozarowski (NHMFL) for his EPR simulation and fit program SPIN, and Prof. Eric Schelter and Ekaterina Lapsheva for collecting SQuID data and for insightful discussions.

Conflicts of interest

There are no conflicts to declare.

Notes and references

1 (*a*) F. F. Puschmann, D. Stein, D. Heift, C. Hendriksen, Z. A. Gal, H.-F. Grützmacher and H. Grützmacher, *Angew. Chem., Int. Ed.*, 2011, **50**, 8420; (*b*) A. R. Jupp and J. M. Goicoechea, *Angew. Chem., Int. Ed.*, 2013, **52**, 10064; (*c*) J. M. Goicoechea and H. Grützmacher, *Angew. Chem., Int. Ed.*, 2018, **57**, 16968; (*d*) F. Tambornino, A. Hinz, R. Köppe and J. M. Goicoechea, *Angew. Chem., Int. Ed.*, 2018, **57**, 8230.
2 L. N. Grant, B. Pinter, B. C. Manor, H. Grützmacher and D. J. Mindiola, *Angew. Chem., Int. Ed.*, 2018, **57**, 1049.
3 L. N. Grant, B. Pinter, B. C. Manor, R. Suter, H. Grützmacher and D. J. Mindiola, *Chem. – Eur. J.*, 2017, **23**, 6272.
4 (*a*) S. Alidori, D. Heift, G. Santiso-Quinones, Z. Benkő, H. Grützmacher, M. Caporali, L. Gonsalvi, A. Rossin and M. Peruzzini, *Chem. – Eur. J.*, 2012, **18**, 14805; (*b*) L. Liu, D. A. Ruiz, F. Dahcheh, G. Bertrand, R. Suter, A. M. Tondreau and H. Grützmacher, *Chem. Sci.*, 2016, **7**, 2335; (*c*) A. R. Jupp, M. B. Geeson, J. E. McGrady and J. M. Goicoechea, *Eur. J. Inorg. Chem.*, 2016, 639; (*d*) S. Yao, Y. Xiong, T. Szilvási, H. Grützmacher and M. Driess, *Angew. Chem., Int. Ed.*, 2016, **55**, 4781; (*e*) Y. Wu, L. Liu, J. Su, J. Zhu, Z. Ji and Y. Zhao, *Organometallics*, 2016, **35**, 1593; (*f*) Y. Xiong, S. Yao, T. Szilvási, E. Ballestero-Martínez, H. Grützmacher and M. Driess, *Angew. Chem., Int. Ed.*, 2017, **56**, 4333; (*g*) T. P. Robinson, M. J. Cowley, D. Scheschkewitz and J. M. Goicoechea, *Angew. Chem., Int. Ed.*, 2014, **54**, 683; (*h*) M. Joost, W. J. Transue and C. C. Cummins, *Chem. Commun.*, 2017, **53**, 10731; (*i*) G.-L. Hou, B. Chen, W. J. Transue, Z. Yang, H. Grützmacher, M. Driess, C. C. Cummins, W. T. Borden and X.-B. Wang, *J. Am. Chem. Soc.*, 2017, **139**, 8922; (*j*) R. J. Gilliard, Jr., R. Suter, E. Schrader, Z. Benkő, A. L. Rheingold, H. Grützmacher and J. D. Protasiewicz, *Chem. Commun.*, 2017, **53**, 12325; (*k*) D. Heift, Z. Benkő and H. Grützmacher, *Dalton Trans.*, 2014, **43**, 5920; (*l*) C. Camp, N. Settineri, J. Lefèvre, A. R. Jupp, J. M. Goicoechea, L. Maron and J. Arnold, *Chem. Sci.*, 2015, **6**, 6379; (*m*) C. J. Hoerger, F. W. Heinemann, E. Louyriac, L. Maron, H. Grützmacher and K. Meyer, *Organometallics*, 2017, **36**, 4351; (*n*) R. J. Gilliard, D. Heift, Z. Benkő, J. M. Keiser, A. L. Rheingold, H. Grützmacher and J. D. Protasiewicz, *Dalton Trans.*, 2018, **47**, 666; (*o*) S. Bestgen, Q. Chen, N. H. Reesa and J. M. Goicoechea, *Dalton Trans.*, 2018, **47**, 13016; (*p*) Y. Mei, D.-J. Wu, J. E. Borger and H. Grützmacher, *Angew. Chem., Int. Ed.*, 2018, **57**, 5512; (*q*) D. W. N. Wilson, A. Hinz and J. M. Goicoechea, *Angew. Chem., Int. Ed.*, 2018, **57**, 2188.
5 B. L. Tran, B. Pinter, A. J. Nichols, C.-H. Chen, F. T. Konopka, R. Thompson, J. Krzystek, A. Ozarowski, J. Telser, M.-H. Baik, K. Meyer and D. J. Mindiola, *J. Am. Chem. Soc.*, 2012, **134**, 13035.
6 See the ESI†.
7 U. J. Kilgore, H. Fan, M. Pink, E. Urnezius, J. D. Protasiewicz and D. J. Mindiola, *Chem. Commun.*, 2009, 4521.
8 F. Basuli, B. C. Bailey, J. C. Huffman, M.-H. Baik and D. J. Mindiola, *J. Am. Chem. Soc.*, 2004, **126**, 1924.
9 T. W. Graham, K. A. Udachin, M. Z. Zgierski and A. J. Carty, *Organometallics*, 2011, **30**, 1382.
10 B. Sieklucka and D. Pinkowicz, *Molecular Magnetic Materials: Concepts and Applications*, 2017, vol. 1.
11 R. Boča, *Coord. Chem. Rev.*, 2004, **248**, 757.
12 R. Boča, Magnetic Parameters and Magnetic Functions in Mononuclear Complexes Beyond the Spin-Hamiltonian Formalism, in *Magnetic Functions Beyond the Spin-Hamiltonian. Structure and Bonding*, ed. D. M. P. Mingos, Springer, Berlin, Heidelberg, 2005, vol. 117, p. 1.
13 J. Krzystek and J. Telser, *Dalton Trans.*, 2016, **45**, 16751.
14 J. Telser, *eMagRes*, 2017, **6**, 207.
15 J. Krzystek, A. Ozarowski and J. Telser, *Coord. Chem. Rev.*, 2006, **250**, 2308.
16 B. L. Tran, J. Krzystek, A. Ozarowski, C.-H. Chen, M. Pink, J. A. Karty, J. Telser, K. Meyer and D. J. Mindiola, *Eur. J. Inorg. Chem.*, 2013, 3916.
17 P. J. Alonso, J. Forniés, M. A. GarcíaMonforte, A. Martín and B. Menjón, *Chem. – Eur. J.*, 2005, **11**, 4713.
18 W. Mowat, A. J. Shortland, N. J. Hill and G. Wilkinson, *J. Chem. Soc., Dalton Trans.*, 1973, 770.